ANZIAM J. 61(2019), 148–160
doi:10.1017/S1446181119000051

ON THE TOPOGRAPHY-DRIVEN VORTICITY PRODUCTION IN SHALLOW LAKES

BALÁZS SÁNDOR✉[1,2], PÉTER TORMA[1], K. GÁBOR SZABÓ[1] and HONG ZHANG[2]

(Received 26 July, 2018; accepted 10 February, 2019; first published online 3 May 2019)

Abstract

We analyse the vorticity production of lake-scale circulation in wind-induced shallow flows using a linear elliptic partial differential equation. The linear equation is derived from the vorticity form of the shallow-water equation using a linear bed friction formula. The features of the wind-induced steady-state flow are analysed in a circular basin with topography as a concave paraboloid, having a quadratic pile in the middle of the basin. In our study, the size of the pile varies by a size parameter. The vorticity production due to the gradient in the topography (and the distance of the boundary) makes the streamlines parallel to topographical contours, and beyond a critical size parameter, it results in a secondary vortex pair. We compare qualitatively and quantitatively the steady-state circulation patterns and vortex evolution of the flow fields calculated by our linear vorticity model and the full, nonlinear shallow-water equations. From these results, we hypothesize that the steady-state topographical vorticity production in lake-scale wind-induced circulations can be described by the equilibrium of the wind friction field and the bed friction field. Moreover, the latter can also be considered as a linear function of the velocity vector field, and hence the problem can be described by a linear equation.

2010 *Mathematics subject classification*: primary 35Q35; secondary 76D17.

Keywords and phrases: vorticity equilibrium, shallow water, linear circulation model, large-scale environmental flow.

1. Introduction

Various forms of the shallow-water vorticity equation have been applied to describe the large-scale horizontal motions and different wave phenomena in oceans, lakes and other water bodies. Depending on the goal of the analysis, various terms of the vorticity equation can be neglected or simplified. For instance, it is not rare that for certain

[1]Department of Hydraulic and Water Resources Engineering, Faculty of Civil Engineering, Budapest University of Technology and Economics, H-1111 Budapest, Hungary;
e-mail: sandor.balazs@epito.bme.hu, torma.peter@epito.bme.hu, szabo.gabor@epito.bme.hu.
[2]Griffith School of Engineering, Griffith University, Queensland 4222, Australia;
e-mail: hong.zhang@griffith.edu.au.

problems the governing equations can be reduced to linear equations [6, 12, 13, 28–30, 33, 34]. Even though nowadays high-speed computers can easily solve nonlinear equation systems, the solution of a linear equation is still faster, and the knowledge about the rates of participation between the terms in a complex vorticity equilibrium is valuable.

The nonlinearity of the shallow-water vorticity equation arises from the curl of the nonlinear acceleration (which is usually manifested in the advection of vorticity and the vortex stretching terms) on the one hand, and the consideration of the bottom friction term as a nonlinear (usually quadratic) function of the velocity vector field on the other. This full nonlinear model can be used in a wide range of shallow flows, such as modelling large scale [24] and small scale [11] transient vortex structures over isolated topographical obstacles, jet flowing through a circular reservoir at low Reynolds number [3] and also computing wind-induced large-scale steady-state circulations in a shallow lake [23]. Zimmerman [37] and Dippner [9] showed the importance of the vorticity advection and stretching terms by modelling transient vortex structures using the characteristic values of certain seabays. However, the large time-scale and steady-state simulations of large vortex structures do not necessarily need to consider all the nonlinear terms or even the eddy viscosity term, as the following examples will show.

The effect of vorticity source from wind stress curl on large-time-scale topographic waves was investigated by Shilo et al. [31, 32], who neglected the eddy viscosity term and used linear bottom friction connection. Laval et al. [20, 21] and Rubbert and Köngeter [25] also neglected the advection of the vorticity, and showed that the bottom stress has larger influence on the vorticity equilibrium than the vortex stretching term analysing a similar problem of Shilo et al. Józsa et al. [15, 16] analysed the effect of the wind stress curl solving the full nonlinear equation, and showed the dominant effect of wind and bottom friction terms on large-scale wind-induced circulations in shallow lakes.

Simons [33, 34] discussed how the basic features of all circulations can be modelled satisfactorily with a linear model of the friction terms. Schwab and Beletsky [30] have compared different nonlinear and linear models and showed the important role of the bottom friction term considered with either quadratic or linear connection (in both cases, the influence of the bottom friction term is of the same magnitude). Csanady [6] described the long-term topographic waves in coastal zones with simple linear vorticity equilibrium between the bottom friction and the Coriolis term. Huang [12] also described waves with linear equilibrium of bottom and wind stresses in a shallow lake, and showed the role of the (linear) bottom friction on the dissipation of the vorticity waves. Jamart [13] described the steady-state wind-driven circulations with linear model of the bottom, wind stresses and the Coriolis term. Schwab [28, 29] used a linear model to generate impulse response functions, and estimated the water-level displacements from wind field data using convolution instead of using any dynamical equations. All these results also confirm that the basic features of large-scale wind-induced circulations can be described by linear models to a certain degree.

In this paper, we are looking at the accuracy of a linear vorticity equilibrium model on the topographical vorticity production in wind-induced circulation of a shallow lake. The topography is considered as a concave paraboloid: a quadratic pile in a quartic basin. The quadratic pile increases by a size parameter. It should be noted here that the full nonlinear vorticity equation involving varying topography in time was deduced by Da et al. [7]. Our goal is to show that the linear vorticity model may describe qualitatively and quantitatively the large-scale features of the steady states corresponding to piles with different sizes. To validate our model, we compare the results with a ratified shallow-flow model which considers the full shallow-water equations, including quadratic bottom friction connection.

2. The vorticity equation

We consider the steady-state vorticity equilibrium between the bottom friction $\boldsymbol{\tau}^b$ and wind-generated surface friction $\boldsymbol{\tau}^w$ fields:

$$\nabla \wedge \frac{\boldsymbol{\tau}^b}{h} = \nabla \wedge \frac{\boldsymbol{\tau}^w}{h}, \tag{2.1}$$

where h describes the water depth with constant surface level

$$\nabla = \Big[\frac{\partial}{\partial x}, \frac{\partial}{\partial y}\Big],$$

and $\wedge$ denotes the curl of planar vector fields. Assuming a linear connection between the bottom friction field and the depth integrated velocity vector field $\mathbf{q}$, we can write

$$\boldsymbol{\tau}^b = C^b \rho \mathbf{q}, \tag{2.2}$$

where ρ is the (constant) density of the water and C^b is a linear friction coefficient with dimension s^{-1}. We introduce the stream function ψ of the depth integrated velocity vector field:

$$\mathbf{q} = \Big[-\frac{\partial \psi}{\partial y}, \frac{\partial \psi}{\partial x}\Big]. \tag{2.3}$$

The wind friction field is assumed to be constant:

$$\boldsymbol{\tau}^w = C^w \rho_{\mathrm{air}} W^2 [\cos\delta, \sin\delta] \tag{2.4}$$

with the dimensionless friction coefficient C^w, wind speed W and wind direction δ. Substituting formulae (2.2)–(2.4) into equation (2.1) and assuming no slip boundary condition results in the following Dirichlet problem on an $\Omega \subset \mathbb{R}^2$ domain:

$$\begin{cases} h\Delta\psi - \nabla h \cdot \nabla\psi = \kappa h\Big(\dfrac{\partial h}{\partial y}\cos\delta - \dfrac{\partial h}{\partial x}\sin\delta\Big) & \text{in } \Omega, \\ \psi = 0 & \text{on } \partial\Omega, \end{cases} \tag{2.5}$$

where

$$\kappa = \frac{C^w \rho_{\mathrm{air}} W^2}{C^b \rho}, \tag{2.6}$$

https://doi.org/10.1017/S1446181119000051 Published online by Cambridge University Press

which has the dimension $\mathrm{m}^2\,\mathrm{s}^{-1}$. Considering

$$\kappa h\Big(\frac{\partial h}{\partial y}\cos\delta - \frac{\partial h}{\partial x}\sin\delta\Big) \in L^2(\Omega) \quad \text{and} \quad \psi \in C^2(\Omega) \cap C(\overline{\Omega}),$$

where $\overline{\Omega} = \Omega \cup \partial\Omega$, we write the weak form of (2.5) as

$$B(\psi, \phi) = F\phi, \quad \text{for all } \phi \in L^2(\Omega), \tag{2.7}$$

with

$$B(\psi, \phi) = \int_\Omega (h\nabla\psi \cdot \nabla\phi + 2\nabla h \cdot \nabla\psi\phi)\, dA$$

and

$$F\phi = -\int_\Omega \kappa h\Big(\frac{\partial h}{\partial y}\cos\delta - \frac{\partial h}{\partial x}\sin\delta\Big)\phi\, dA,$$

where $\phi \in L^2(\Omega)$ is a test function and dA is the area element in $\mathbb{R}^2$.

3. Bifurcating vortex solution for varying topography

3.1. Depth function We are assuming a circular-shaped shallow lake with the depth function

$$h = 1 - 10^{-11} r^2(r^2 - \varepsilon^2), \quad \varepsilon \in (0, 700), \tag{3.1}$$

which describes the depth variation of a convex quartic basin and a concave quadratic pile added to the basin with a size parameter ε and $r^2 = x^2 + y^2$. The topography can be written in the form

$$b = 10^{-11} r^2(r^2 - \varepsilon^2).$$

Figure 1 shows the topography and the constant water level.

The radius of the lake is the first root of the depth function (3.1)

$$R = \sqrt{\frac{\varepsilon^2 + \sqrt{\varepsilon^4 + 4 \times 10^{11}}}{2}}, \tag{3.2}$$

and

$$R|_{\varepsilon=0} = 562.34\ \mathrm{m}, \quad R|_{\varepsilon=700} = 803.13\ \mathrm{m}.$$

The depth function (3.1) has nonnegative extrema at $r = 0$ and $r = \varepsilon/\sqrt{2}$, which are the top and the bottom of the pile, respectively, and an inflexion point in between at $r = \varepsilon/\sqrt{6}$.

The water depth at the top of the pile and at the maximal depth is

$$h(0) = 1, \quad h(\varepsilon/\sqrt{2}) = 1 + \frac{\varepsilon^4}{4 \times 10^{11}},$$

respectively. Hence, if we denote the maximal depth by H then

$$H|_{\varepsilon=0} = 1.00\ \mathrm{m}, \quad H|_{\varepsilon=700} = 1.60\ \mathrm{m}.$$

https://doi.org/10.1017/S1446181119000051 Published online by Cambridge University Press

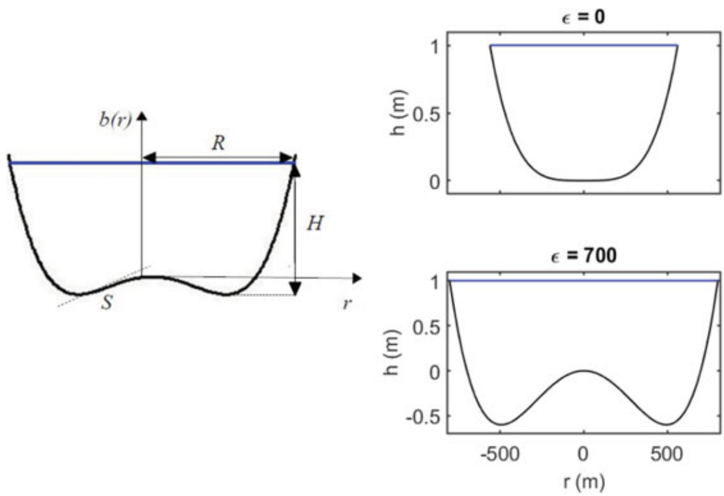

FIGURE 1. Topography of a convex quartic basin with a concave quadratic pile with constant water level generally (left), and for $\varepsilon = 0$ and $\varepsilon = 700$ specifically (right).

We measure the shallowness of the lake as the quotient of its depth and diameter:

$$\frac{H}{2R}\Big|_{\varepsilon=0} = 0.002 \ll 1, \quad \frac{H}{2R}\Big|_{\varepsilon=700} = 0.002 \ll 1.$$

The $\varepsilon = 0$ limit is a convex quartic basin; the flow pattern in such a case with a uniform wind friction field is a pair of counter-rotating circulating domains [12, 15, 16]. Vorticity is produced with increasing ε around the centre with radius ε. To measure this production, we assume that the characteristic depth gradient S is the local depth gradient maximum at the inflexion point of the depth function:

$$S = h_r(\varepsilon/\sqrt{6}) = \frac{\sqrt{6}}{45 \times 10^{10}}\varepsilon^3,$$
$$S|_{\varepsilon=700} = 0.002.$$

3.2. Galerkin discretization and parameter quantification Expanding the weak form (2.7) in polar coordinates (r, φ) leads to

$$\int_0^{2\pi}\int_0^R \{h(\partial_r\psi\partial_r\phi + r^{-2}\partial_\varphi\psi\partial_\varphi\phi) + \partial_r h\phi(2\partial_r\psi + \kappa h\sin(\varphi - \delta))\}r\,dr\,d\varphi = 0, \quad (3.3)$$

where both $h(r)$ and R depend on ε parametrically according to formulae (3.1) and (3.2), respectively. We seek the solution with the Galerkin procedure (see [26] for general details) in the form

$$\psi_k = \sum_{j=1}^{k} c_j\hat{\psi}_j(r, \varphi) = \sum_{j=1}^{k} c_j\varrho_j(r)\sin(\varphi - \delta), \quad c_j \in \mathbb{R}. \quad (3.4)$$

https://doi.org/10.1017/S1446181119000051 Published online by Cambridge University Press

The polar angle related higher harmonics should not be taken into account, since the topography is independent of the polar angle. The radial basis functions are constructed by a Gram–Schmidt process from the sequence $r(r-R)$, $r^2(r-R)$, $r^3(r-R)\ \ldots$, in order to naturally satisfy the boundary conditions. We use the following three basis functions to obtain the solution:

$$\begin{aligned}\varrho_1 &= \sqrt{\frac{30}{R^5}}\, r(r-R),\\ \varrho_2 &= \sqrt{\frac{210}{R^7}}\, r(2r^2-3rR+R^2),\\ \varrho_3 &= \sqrt{\frac{90}{R^9}}\, r(r-R)(14r^2-14rR+3R^2),\end{aligned} \tag{3.5}$$

for which

$$\int_0^R \varrho_i\varrho_j\,dr = \delta_{ij}, \quad i=1,\ldots,k,\ j=1,\ldots,k,$$

where δ_{ij} is the Kronecker delta symbol. The radial elements ensure that the boundary condition $\psi = 0$ on $\partial\Omega$ is satisfied, which now reads

$$\varrho_i(R) = 0, \quad i=1,\ldots,k.$$

We determine κ using formula (2.6). The density of air and water are

$$\rho_{\mathrm{air}} = 1.2\ \mathrm{kg\ m^{-3}}, \quad \rho = 1000\ \mathrm{kg\ m^{-3}}, \tag{3.6}$$

respectively. A specific wind speed and wind friction coefficient are chosen in accordance with existing work in the literature [5, 17, 35, 36] as

$$W = 3\ \mathrm{m\ s^{-1}}, \quad C^w = 1.5\times 10^{-3}, \tag{3.7}$$

respectively. Let the bottom friction coefficient be

$$C^b = 2\times 10^{-4}\ \mathrm{s^{-1}}, \tag{3.8}$$

in agreement with Simons [33]. Substituting (3.6)–(3.8) into formula (2.6) yields

$$\kappa = 0.08\ \mathrm{m^2\ s^{-1}}, \tag{3.9}$$

and we are specifying northern wind,

$$\delta = \frac{\pi}{2}. \tag{3.10}$$

For the sake of simplicity, we identify the test functions ϕ of the weak form (3.3) with the basis elements in V_k:

$$\phi_i = \hat{\psi}_i, \tag{3.11}$$

https://doi.org/10.1017/S1446181119000051 Published online by Cambridge University Press

described by formulae (3.4)–(3.5). Using the parameter (3.9) and the wind direction (3.10) and considering the basis functions (3.4)–(3.5) and condition (3.11), the weak form (3.3) leads to the following system of algebraic equations for the c_j:

$$\pi \int_0^R r\,dr\Big(h \sum_{j=1}^{k} c_j \frac{\partial \varrho_j}{\partial r}\frac{\partial \varrho_i}{\partial r} + \frac{\partial h}{\partial r}\varrho_i\Big(2\sum_{j=1}^{k} c_j \frac{\partial \varrho_j}{\partial r}\Big) + 0.08 \cdot h + r^{-2} \sum_{j=1}^{k} c_j \varrho_j \varrho_i\Big) = 0. \tag{3.12}$$

We are left with a one-parameter (ε) family of solutions of the form (3.4) with c_j coefficients resulting from equation (3.12). For $\varepsilon = 0$, we find a simple vortex pair solution arranged symmetrically with respect to the wind direction. With increasing ε, the streamlines develop the tendency to gradually align with the circular topographical contour lines around the centre. The range of modified streamlines gets wider with the increase in ε, until a critical parameter value $\varepsilon_{\mathrm{crit}}$ is reached. At this parameter value, a qualitative change occurs in the flow pattern: a small secondary vortex pair emerges at the centre. This secondary flow structure gradually grows with further increase in ε.

The above scenario indicates the existence of a steady-state bifurcation in the system. Indeed, floating-point root approximation for various ε confirms that a new positive real root of the polynomial (3.4) appears at

$$\varepsilon_{\mathrm{crit}} = 436. \tag{3.13}$$

Note that Chen [4] found Hopf bifurcations in wind-induced unsteady quasi-geostrophic flows. In contrast, the bifurcation parameter (3.13) characterizes the steady-state flow patterns. The solution is a single vortex pair or a double vortex pair, if $\varepsilon < \varepsilon_{\mathrm{crit}}$ or $\varepsilon > \varepsilon_{\mathrm{crit}}$, respectively.

4. Comparing the results with a nonlinear shallow-flow model

In order to show that lake-scale circulation pattern and vortex evolution can be reliably estimated by our simple linear model, we compare our results with flow fields calculated by a full nonlinear model. The full model solves the incompressible Reynolds-averaged shallow-water equations invoking the assumption of Boussinesq (see [1] for details) and of hydrostatic pressure without neglecting advective and eddy viscosity terms, as well as applying a nonlinear bed friction formula. The model consists of a continuity equation and two momentum equations for the two horizontal depth-averaged velocity components, respectively. We chose the Mike21 software by DHI [8] to solve the dynamic shallow-water equations numerically. Mike21 had been previously applied extensively, and successfully verified in many wind-driven coastal, estuarine and lake environments [19, 22, 27]. Therefore, we give only a brief description of the solver here, and for further details we refer to the model documentation [8]. The numerical solution is obtained by an element centred, Godunov-type finite-volume scheme [8, 10] with second order accurate time integration. The maximum time-step was set to 10 s to ensure the Courant–Friedrich–Levy stability condition [1]. The spatial domain is discretized with an unstructured

https://doi.org/10.1017/S1446181119000051 Published online by Cambridge University Press

triangular mesh which is able to capture complex bathymetry and curved shorelines. The spatial resolution is determined by a mesh refinement test in order to obtain mesh-independent results. The applied cell size was 25 m.

The wind stress acting on the water surface is determined in the same way as is done by the linear model, using formula (2.4) with an aerodynamic drag coefficient with the same value as (3.7). The extra stress terms arising from Reynolds-averaging are calculated by eddy viscosity concept using the Smagorinsky scheme [1] with a coefficient of 0.28.

For bed friction, we apply in the model Manning's formulation which uses roughness coefficient n with dimension s $\mathrm{m}^{-1/3}$, and the bottom shear stress is related to square of depth-averaged velocity. In order to approximate the bed friction fields of the two models to each other, we can match bottom shear stresses through their formulae (since neither the linear nor the quadratic coefficients have tensorial properties [14]). If we denote the depth-averaged velocity vector field by $\mathbf{v}$, the linear bottom friction expression (2.2) takes the form

$$\boldsymbol{\tau}^b = C^b \rho \mathbf{q} = C^b \rho h \mathbf{v}. \tag{4.1}$$

The quadratic bottom friction law reads

$$\boldsymbol{\tau}^b = C^f \rho \mathbf{v} |\mathbf{v}|, \tag{4.2}$$

where the quadratic drag coefficient C^f is calculated by Manning's formula,

$$C^f = g n^2 h^{-1/3},$$

in which $g = 9.81$ m s^{-2} is the gravitational acceleration, and n is the roughness coefficient. Equating the friction formulae (4.1)–(4.2) and substituting the depth variations with an average depth $\bar{h} = 1$ m and the depth-averaged velocities with an average value $|\bar{\mathbf{v}}| = 0.02$ m s^{-1} according to the topography (3.1) and the results of the linear model simulation, respectively, we obtain the roughness coefficient

$$n = 0.032 \text{ s m}^{-1/3}. \tag{4.3}$$

We use this value (4.3) in the nonlinear model, which is a typical value for roughness coefficient for similar problems [8, 18] as well as the linear friction coefficient (3.8).

The results show good quantitative and qualitative correspondence. The streamline pattern can be viewed for $\varepsilon = 0$ and $\varepsilon = 700$ in Figures 2 and 3, respectively. Since the solution is a vortex pair symmetric to the y-axis, one vortex from the vortex pair is shown for each model for the sake of comparison. Considering the streamfunction values, a small deviation can be seen which is related to the different bed friction formulations which were equaled via lake-averaged velocity and depth, as mentioned above. The sign of the deviation is different in the two plotted cases. According to a sensitivity analysis, these differences cannot be reduced by further friction coefficient calibration.

Since the linear model assumes a horizontal water surface (rigid-lid approximation) and the basin is rotationally symmetric, the estimated streamline patterns are also

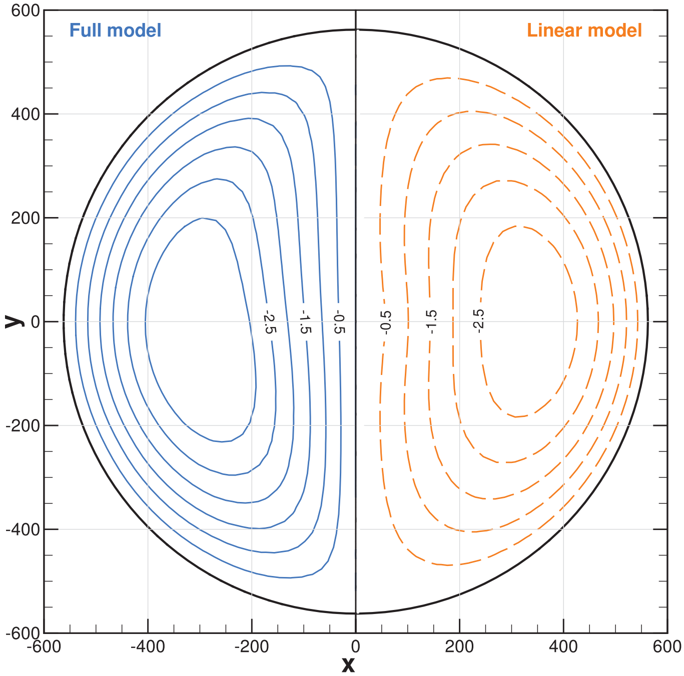

FIGURE 2. Streamfunction representation of the circulation pattern for $\varepsilon = 0$. Left: the solution of the nonlinear model (continuous). Right: the solution of the linear model (dashed).

symmetric to the x-axis. In contrast, the full model is not able to apply the rigid-lid approximation, thus the water surface is tilted from the initial horizontal level, that is, the water level increases (decreases) on the leeward (windward) shore. Surface-level deviations are very low (less than 1 cm) at the north (windward) and south (leeward) ends of the basin. Nevertheless, as a result, in case of northerly wind, lake-scale circulation patterns (both primary and secondary vortices) obtained by the full model are not symmetrical to the x-axis.

To determine the critical ε-value of the second vortex pair and the locations of vortex cores along the basin's radius, 15 cases were modelled by the full model. In these 15 cases, ε varies from 0 to 700 in steps of 100, and in steps of 10 from 420 to 450 to gain more detailed insight close to the critical value of ε, when the formation of the second vortex pair occurs. Streamline functions are calculated from the steady-state velocity fields determining first its curl, and then solving a Poisson equation with a finite-element method on the same mesh.

The bifurcation of the vortex pattern appears in the solution of the nonlinear model as well with

$$\varepsilon_{\text{crit}} = 423.$$

Figure 4 shows the positions of the vortex centres. The appearance of the second vortex pair and the evolution of the vortex cores as a function of ε shows good qualitative

https://doi.org/10.1017/S1446181119000051 Published online by Cambridge University Press

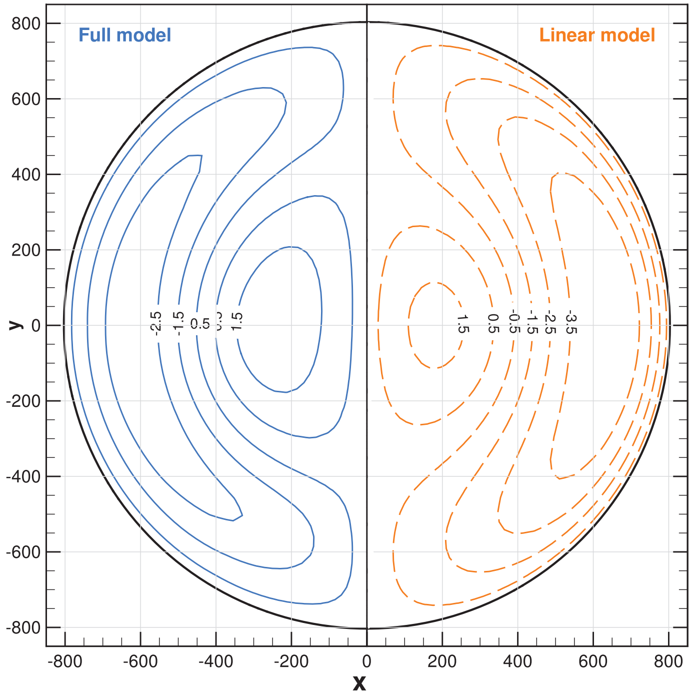

FIGURE 3. Streamfunction representation of the circulation pattern for $\varepsilon = 700$. Left: the solution of the nonlinear model (continuous). Right: the solution of the linear model (dashed).

agreement between the two models. The difference in the exact positions may arise from neglecting all nonlinearities in our model. However, the greatest difference is still less than 10% compared to the radius of the lake.

5. Conclusion

We analysed the evolution of a secondary vortex pair due to topographical vorticity production, away from the boundary in a shallow lake flow generated by uniform wind stress field. If we consider the difference between the two mathematical models that we have compared, the compliance of the results is good; the large-scale features of the problem can be modelled satisfactorily with a linear vorticity equation.

For calculating the steady-state solutions, 10–20 min computation time was needed with the full nonlinear model, while the running time of the linear model was just a few seconds. Beside shallow lakes and reservoirs, where knowing the circulation patterns is essential for many environmental reasons, our model can also be a useful tool to support the design of stormwater ponds. For stormwater or retention ponds, wind and topography might determine the large-scale circulation pattern and the resident time in the pond, from which the sediment retention capability can be evaluated [2]. Also, our model can provide quick estimates of basin-scale circulation patternx for various

https://doi.org/10.1017/S1446181119000051 Published online by Cambridge University Press

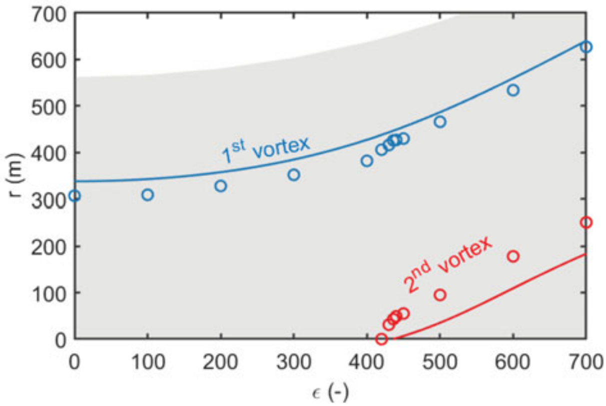

FIGURE 4. Vortex centres calculated with the linear model (continuous lines) and with the nonlinear model (circles) as a function of the size parameter (ε). Centre locations are measured from the centre of the basin. The area shaded grey represents the radius of the lake.

topographies and wind directions, from which the residence time distribution in the pond can be calculated in order to find an ideal geometry and size.

In order to apply our model to such problems, it is important to consider a realistic topography and the effect of the inhomogeneous wind stress field.

Acknowledgements

The scholarship of B. Sándor is covered by Erasmus Mundus PANTHER–Pacific Atlantic Network for Technical Higher Education and Research exchange programme. The research reported in this paper was also supported by the FIKP grant of EMMI in the frame of the Water Sciences & Disaster Prevention research area of BME (BME FIKP-VÍZ).

References

[1] M. B. Abbot and D. R. Basco, *Computational fluid dynamics, an introduction for engineers* (Longman Group, Harlow, 1989).

[2] H. O. Andradóttir and M.-L. Mortamet, "Impact of wind on storm-water pond hydraulics", *J. Hydraul. Eng.* **142** (2016) Id 04016034; doi:10.1061/(ASCE)HY.1943-7900.0001150.

[3] A. G. L. Borthwick and E. T. Kaar, "Shallow flow modelling using curvilinear depth-averaged stream function and vorticity transport equations", *Int. J. Numer. Methods Fluids* **17** (1993) 417–445; doi:10.1002/fld.1650170506.

[4] Z. M. Chen and W. G. Price, "Bifurcating periodic solutions of wind-driven circulation equations", *J. Math. Anal. Appl.* **304** (2005) 783–796; doi:10.1016/j.jmaa.2004.09.062.

[5] B. W. Chubarenko, Y. Wang, I. Chubarenko and C. Hutter, "Wind-driven current simulations around the Island Mainau (Lake Constance)", *Ecol. Modell.* **138** (2001) 55–73; doi:10.1016/S0304-3800(00)00393-8.

[6] G. T. Csanady, "The arrested topographic wave", *J. Phys. Oceanogr.* **8** (1978) 47–62; doi:10.1175/1520-0485(1978)008<0047:TATW>2.0.CO;2.

[7] C. Da, B. Shen, P. C. Yan, D. Ma and J. Song, "The shallow water equation and the vorticity equation for a change in height of the topography", *PLoS ONE* **12** (2017) e0178184; doi:10.1371/journal.pone.0178184.

[8] Danish Hydraulic Institute, *MIKE 21 flow model FM hydrodynamic and transport module* (Danish Hydraulic Institute for Water and Environment, Horsholm, 2011).

[9] J. W. Dippner, "Vorticity analysis of transient shallow water eddy fields at the river plume front of the River Elbe in the German Bight", *J. Mar. Syst.* **14** (1998) 117–133; doi:10.1016/S0924-7963(97)00008-0.

[10] J. H. Ferziger and M. Peric, *Computational methods for fluid dynamics* (Springer, Berlin, 2002).

[11] E. A. Hansen and L. Arneborg, "The use of a discrete Vortex model for shallow water flow around islands and coastal structures", *Coast. Eng.* **32** (1997) 223–246; doi:10.1016/S0378-3839(97)81751-6.

[12] J. C. K. Huang and J. H. Saylor, "Vorticity waves in a shallow basin", *Dyn. Atmos. Ocean.* **6** (1982) 177–196; doi:10.1016/0377-0265(82)90023-9.

[13] B. M. Jamart and J. Ozer, "Comparison of 2-D and 3-D models of the steady wind-driven circulation in shallow waters", *Coast. Eng.* **11** (1987) 393–413; doi:10.1016/0378-3839(87)90020-2.

[14] H. L. Jenter and O. S. Madsen, "Bottom stress in wind-driven depth-averaged coastal flows", *J. Phys. Oceanogr.* **19** (1989) 962–974; doi:10.1175/1520-0485(1989)019<0962:BSIWDD>2.0.CO;2.

[15] J. Józsa, "On the internal boundary layer related wind stress curl and its role in generating shallow lake circulations", *J. Hydrol. Hydromech.* **62** (2014) 16–23; doi:10.2478/johh-2014-0004.

[16] J. Józsa, T. Krámer, E. Napoli and G. Lipari, "Sensitivity of wind-induced shallow lake circulation patterns on changes in lakeshore land use", *EGU Gen. Assem. 2006* **8** (2006) 1–2; EGU06-A-00786.

[17] N. Kimura, C. Wu, J. A. Hoopes and A. Tai, "Diurnal dynamics in a small shallow lake under spatially nonuniform wind and weak stratification", *J. Hydraul. Eng.* **142** (2016); Id 04016047; doi:10.1061/(ASCE)HY.1943-7900.0001190.

[18] T. Krámer and J. Józsa, "An adaptively refined, finite-volume model of wind-induced currents in Lake Neusiedl", *Period. Polytech.* **49** (2005) 111–136; https://pp.bme.hu/ci/article/view/575.

[19] T. Krámer, J. Józsa and P. Torma, "Large-scale mixing of water imported into a shallow lake", *Proc. 3rd Int. Symp. on Shallow Flows,* Iowa City, IO, USA, 4–6 June 2012, (eds G. Constantinescu and H. J. Fernando), available at http://real.mtak.hu/17101/.

[20] B. Laval and J. Imberger, "Modelling circulation in lakes: Spatial and temporal variations", *Limnol. Oceanogr.* **48** (2003) 983–994; doi:10.4319/lo.2003.48.3.0983.

[21] B. Laval, J. Imberger and A. N. Findikakis, "Dynamics of a large tropical lake: Lake Maracaibo", *Aquat. Sci.* **67** (2005) 337–349; doi:10.1007/s00027-005-0778-1.

[22] Y. Li, Q. Zhang, J. Yao and A. D. Werner, "Hydrodynamic and hydrological modelling of the Poyang Lake Catchment System in China", *J. Hydrol. Eng.* **19** (2014) 607–616; doi:10.1061/(ASCE)HE.1943-5584.0000835.

[23] S. Liu, Q. Ye, S. Wu and M. J. F. Stive, "Horizontal circulation patterns in a large shallow lake: Taihu Lake, China", *Water* **10** (2018) 792; doi:10.3390/w10060792.

[24] M. J. Park and D. P. Wang, "Tidal vorticity over isolated topographic features", *Cont. Shelf Res.* **14** (1994) 1583–1599; doi:10.1016/0278-4343(94)90091-4.

[25] S. Rubbert and J. Köngeter, "Measurements and three-dimensional simulations of flow in a shallow reservoir subject to small-scale wind field inhomogeneities induced by sheltering", *Aquat. Sci.* **67** (2005) 104–121; doi:10.1007/s00027-004-0719-4.

[26] S. Salsa, *Partial differential equations in action* (Springer, Cham, 2015).

[27] J. H. Schoen, D. D. Stretch and K. Tirok, "Wind-driven circulation patterns in a shallow estuarine lake: St Lucia, South Africa", *Estuar. Coast. Shelf Sci.* **146** (2014) 49–59; doi:10.1016/j.ecss.2014.05.007.

[28] D. J. Schwab, "Simulation and forecasting of Lake Erie storm surges", *Month. Weath. Rev.* **106** (1978) 1476–1487; doi:10.1175/1520-0493(1978)106<1476:SAFOLE>2.0.CO;2.

[29] D. J. Schwab, "An inverse method for determining wind stress from water-level fluctuations", *Dyn. Atmos. Oceans* **6** (1982) 251–278; doi:10.1016/0377-0265(82)90032-X.

[30] D. J. Schwab and D. Beletsky, "Relative effects of wind stress curl, topograpy, and stratification on large-scale circulation in Lake Michigan", *J. Geophys. Res.* **108** (2003); C2 3044; doi:10.1029/2001JC001066.

[31] E. Shilo, "Wind spatial variability and topographic wave frequency", *J. Phys. Oceanogr.* **38** (2008) 2085–2096; doi:10.1175/2008JPO3886.1.

[32] E. Shilo, Y. Ashkenazy, A. Rimmer, S. Assouline, P. Katsafados and Y. Mahrer, "Effect of wind variability on topographic waves: Lake Kinneret case", *J. Geophys. Res.* **112** (2007); C1 2024; doi:10.1029/2007JC004336.

[33] T. J. Simons, "Circulation models of lakes and inland seas", in: *Canadian bulletin of fisheries and aquatic sciences* (Dept. of Fisheries and Oceans, Ottawa, 1980).

[34] T. J. Simons, "Reliability of circulation models", *J. Phys. Oceanogr.* **15** (1985) 1191–1204; doi:10.1175/1520-0485(1985)015<1191:ROCM>2.0.CO;2.

[35] P. Torma and C. H. Wu, "Temperature and circulation dynamics in a small and shallow lake: effects of weak stratification and littoral submerged macrophytes", *Water* **11** (2019) 128; doi:10.3390/w11010128.

[36] J. Wu, "Wind–stress coefficients over sea surface from breeze to hurricane", *J. Geophys. Res.* **87** (1982) 9704; doi:10.1029/JC087iC12p09704.

[37] J. T. F. Zimmerman, "Topographic generation of residual circulation by oscillatory (tidal) currents", *Geophys. Astrophys. Fluid Dyn.* **11**(1) (1978) 35–47; doi:10.1080/03091927808242650.